Advanced Study of Switchable Spin Crossover Compounds

Gavin Craig

ADVANCED STUDY OF SWITCHABLE SPIN CROSSOVER COMPOUNDS

Universitat de Barcelona

Facultat de Química

Departament de Química Inorgànica

Programa de Doctorat: Química Inorgànica Molecular

Grup de Magnetisme i Molècules Funcionals

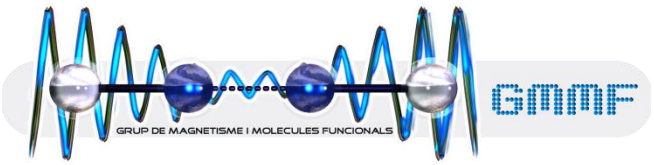

Gavin Craig

Director: Dr. Guillem Aromí Bedmar, Departament de Química Inorgànica

Tutor: Dr. Santiago Alvarez Reverter, Departament de Química Inorgànica

Contents

Chapter 6: The effect of solvent and anion variation on $[Fe(H_4L)_2](ClO_4)_2 \cdot H_2O \cdot 2(CH_3)_2CO$

6.0 Introduction

In the preceding Chapters, the SCO properties of compound $[Fe(H_4L)_2](ClO_4)_2 \cdot H_2O \cdot 2(CH_3)_2CO$, **1**, were understood on the basis of the structural data for the different phases in which the system could be observed. The crystallographic studies allowed explanations to be proposed for the asymmetric hysteresis loop and the disparate relaxation kinetics of meta-stable states of **1**. This was justified by the supramolecular relationship between the lattice's spin-active components ($[Fe(H_4L)_2]^{2+}$ cations) and its spin-inactive entities (anions, solvent molecules).

In this context, changing the solvent molecules used in the synthesis and/or the crystallisation of the compounds, may alter the supramolecular connectivity that links the lattice components, and with it the presented magnetic properties. This approach is common in SCO research.[1-7] For example, Hasegawa *et al*. recently described how the compound $[Fe(E\text{-dpsp})_2](BF_4)_2 \cdot Sx$ (where *E*-dpsp = *E*-2,6-bis(pyrazol-1-yl)-4-styrylpyridine) displayed a hysteretic transition when Sx = acetone; was fully HS and devoid of SCO when Sx = acetonitrile; and was fully LS with no SCO when Sx = diethyl ether.[8] Using the observed crystal structures, they explained these different behaviours as due to the lack of significant intermolecular interactions between the cations in the system, and the cooperativity of the acetone-containing compound to be due to a $\pi\cdots\pi$ interaction and a specific H···H short contact.

Likewise, anion variation can modulate the magnetic properties of SCO systems.[9-14] In fact, Wei and co-workers were able to establish a near-linear relationship between the anion size and the SCO temperature in a family of 1D chain compounds of the general formula $[Fe(tpa)(N(CN)_2)]_x \cdot Y$, where Y corresponds to the anion, and tpa = tri(2-pyridylmethyl)amine.[15] That work followed up a previous study by the same group of another tpa-based system where solvents were used to tune spin transitions via vapour exchange experiments.[16]

In this Chapter the effect of both anion and solvent variation on the magnetic properties of derivatives of **1** will be discussed, and framed in terms of the structural impact these modifications impart. Eight compounds have been thus obtained, and the availability of

structural data has allowed the rationalisation of their magnetic properties with respect to compound **1**.

6.1 Synthesis

The synthetic approach to obtain the compounds described in this Chapter is similar to that employed for **1**, varying slightly in certain parameters to investigate the effect that changing the anion, the reaction solvent, or the crystallisation conditions (see Table 6.1), has on the structural and magnetic properties of the cation $[Fe(H_4L)_2]^{2+}$. Compound **2** was initially formed as a by-product in the same synthesis which led to **1**, as small, air-sensitive orange crystals which crystallised on the sides of the test tube. It was found that by adding a drop of H_2O to the mother liquor, or by gently moving the tube to accelerate the diffusion of the layers, the formation of **1** could be suppressed, bringing about the exclusive crystallisation of **2**. X-ray diffraction studies revealed the molecular composition to be $[Fe(H_4L)_2](ClO_4)_2 \cdot Et_2O \cdot 3(CH_3)_2CO$, later confirmed by elemental analysis. This amounts to the insertion of a further molecule of acetone in the crystal lattice, together with one of diethyl ether, and the removal of H_2O. By substituting the precipitating solvent layers of **1**, replacing diethyl ether with dichloromethane, small orange crystals of **3** were yielded, however the process was slower with respect to the original procedure, taking two months to crystallise. While the composition of compound **3**, $[Fe(H_4L)_2](ClO_4)_2 \cdot H_2O \cdot 2(CH_3)_2CO$, coincides with that of **1**, the magnetic properties are demonstrably different, as is the morphology of the crystals, justifying their treatment as two distinct systems.

Compound	Ligand	Anion	Reaction Solvent	Crystallisation
2	H_4L	ClO_4^-	Acetone	Layer, Diethyl ether
3		ClO_4^-	Acetone	Layer, Dichloromethane
4		ClO_4^-	Ethanol	Layer, Hexane
5		ClO_4^-	Propan-2-ol	Layer, Diethyl Ether
6		ClO_4^-	Nitromethane	Slow evaporation
8		BF_4^-	Acetone	Layer, Hexane
9		$CF_3SO_3^-$	Acetone	Layer, Hexane
10		SCN^-	MeOH	Slow evaporation

Table 6.1: Reaction conditions for the compounds described in Chapter 6.

Changing the solvent medium in which the reaction takes place led to the synthesis of compounds **4**, **5**, and **6**. Using ethanol (**4**) or isopropanol (**5**) before layering with hexane (**4**) or diethyl ether (**5**) brought about the crystallisation of $[Fe(H_4L)_2](ClO_4)_2 \cdot 4C_2H_5OH$ (**4**) and $[Fe(H_4L)_2](ClO_4)_2 \cdot 2C_3H_7OH$ (**5**), where the presence of the reaction solvent in the crystal structure modifies the crystal packing with respect to the terpyridine embrace of **1**. While these reactions required the presence of a precipitating solvent, the synthesis with nitromethane was left to slowly evaporate, which led to the formation of compound **6** $[Fe(H_4L)_2](ClO_4)_2 \cdot 2CH_3NO_2 \cdot 2H_2O$.

More significant effects were observed on changing the charge-balancing anion of the Fe(II) salt used. On performing the synthesis of the compound $[Fe(H_4L)(H_2LBF_2)](BF_4) \cdot 5C_3H_6O \cdot 2H_2O$, **8**, it was anticipated that the tetrafluoroborate anion would fulfil a structural role similar to that of the perchlorate anion in **1**. However, it was found that the anion was not inert in the reaction conditions, inducing the fluoroboration of one of the H_4L ligands coordinated to the metal, via the addition of a "BF_2" fragment between the O− and the N−atoms of one phenol group and its adjacent pyrazolyl ring. Consequently, the cation is monovalent, since the H_2LBF_2 ligand is anionic. Although this transformation was unexpected, there is one precedent in the literature, involving the fluoroboration of a Schiff-base that was coordinated to Ni(II).[17] This contrasts with the case of the triflate anion in compound **9** of the formula $[Fe(H_4L)_2](CF_3SO_3)_2 \cdot 3(CH_3)_2CO$. Here, the terminal fluorine atoms of the triflate do act in a similar fashion to the perchlorate anions observed previously.

The use of $Fe(NCS)_2$ brought about more unexpected outcomes. The resolution of the crystals obtained by reaction of this salt with H_4L in the presence of ascorbic acid revealed that oxidative cleavage of the anti-oxidant formed the oxalate anion, allowing the oxidation of Fe(II) to Fe(III) to occur.[18] The oxalate anion then bridged the metal ions, to form the dinuclear heptacoordinated Fe(III) compound $[Fe_2(H_4L)_2(ox)(NCS)_4] \cdot MeOH$ (**10**). As this process was serendipitous, a more controlled route was designed for the compound, adding oxalic acid directly to the reaction, in the absence of ascorbic acid, leaving the synthesis to proceed according to the following balanced equation:

$$2Fe(NCS)_2 + 2H_4L + H_2ox + {}^1/_2O_2 \rightarrow [Fe_2(H_4L)_2(ox)(NCS)_4] + H_2O$$

This approach did in fact lead to the same compound as the initial attempt, demonstrated by elemental analysis and IR spectroscopy. Compound **10**, therefore, represents the most radical departure from the other iron compounds described in the thesis.

6.2 Single crystal X-ray diffraction study of $[Fe_2(H_4L)_2(ox)(NCS)_4]$

The crystal structure of the neutral molecule $[Fe_2(H_4L)_2(ox)(NCS)_4]$ in **10** is shown in Figure 6.1. The compound crystallises in the monoclinic space group $P2_1/c$ (see Table 6.2), and the unit cell consists of four molecules of the dinuclear complex, and 4 lattice molecules of MeOH. The molecule is composed of two heptacoordinate Fe(III) ions, present due to the oxidation of the Fe(II) salt employed in the synthesis, bridged by an oxalate ligand that is formed either by the degradation of ascorbic acid or by the deprotonation of oxalic acid, depending on the synthetic route chosen. The metal ions are related by an inversion centre, and the distance between them is 5.702(2) Å. With two

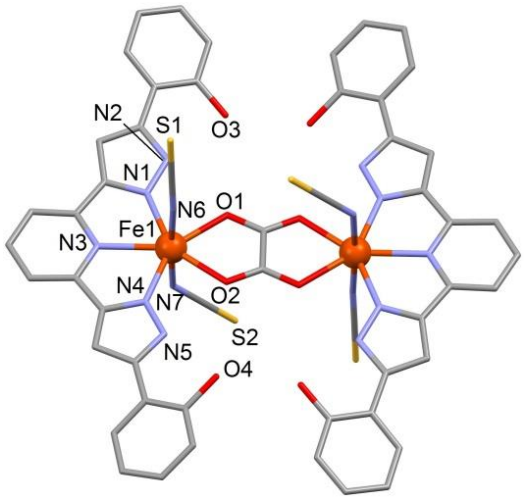

Figure 6.1: Representation of the molecular structure of the dinuclear entity in **10**. The hydrogen atoms have been omitted for clarity, and only the crystallographically unique heteroatoms have been labelled.

equatorial positions occupied by the oxygen atoms of the oxalate, the three remaining such sites are filled by the three central nitrogen donors of the neutral H_4L ligand, and the two axial positions are filled by the nitrogen atoms of the thiocyanate anion, leading to a pentagonal bipyramidal coordination sphere for both Fe(III) ions. The Fe-N and Fe-O bond distances are indicative of a HS Fe(III) species, which is confirmed by the magnetic measurements. The *cis*- angles formed in the basal plane range from 69.2(2) to 74.4(2)°,

lying close to the value of 72° for an ideal pentagon. The thiocyanate ions are coordinated in two different modes, although both through the nitrogen atoms: an almost linear mode, in which the Fe-N6-S1 angle measures 168.0(2)°, and another more heavily distorted coordination mode with an associated Fe-N7-S2 angle of 137.4(2)°. The linking of the two paramagnetic ions via an oxalate bridge makes the magnetic study of the superexchange interaction possible.

Compound	10
T/K	150(2)
crystal system	Monoclinic
space group	$P2_1/c$
a/Å	11.493(3)
b/Å	23.530(5)
c/Å	10.094(2)
α/°	90
β/°	109.62(3)
γ/°	90
V/Å^3	2571.2(11)
μ/mm^{-1}	0.926
reflections collected	2970
R1 (all data)	0.0620
wR2 (all)	0.1874
S	1.03
av. Fe-N/Å	2.124
av. Fe-O/Å	2.174

Table 6.2: Crystallographic data and selected structural parameters for compound **10**.

6.3 Magnetic properties (I)

To characterise the magnetic coupling conducted through the bridging moiety, bulk magnetic susceptibility measurements were performed on a polycrystalline sample of **10** in the temperature range 2 to 300 K under a constant magnetic field of 5 kG. The data are shown in Figure 6.2 as a graph of χT *vs.* the temperature *T*. The value of χT at 300 K is 8.0 $cm^3mol^{-1}K$, slightly lower than that predicted for two independent HS Fe(III) ions (*S*

= 5/2; 8.75 $cm^3mol^{-1}K$, g = 2.0).[19] On lowering the temperature, χT decreases until reaching zero at 2 K, consistent with antiferromagnetic exchange interactions between the Fe(III) ions. Analysing the data with the Van Vleck equation for two exchanged coupled Fe(III) ions, based on the Hamiltonian $H = -2JS_1S_2$ yielded the best fit line shown in Figure 6.2, which corresponds to a coupling constant J of –3.9 cm^{-1}, for a g value of 2.0.

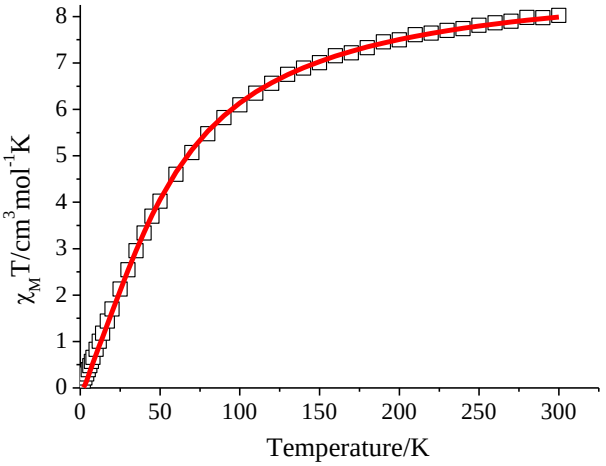

Figure 6.2: Plot of χT *vs*. T for **10**. The solid line corresponds to a fit of the experimental data.

Comparison of the magnetic properties is hindered by the lack of similar systems; there is only one precedent for an oxalate-bridged, heptacoordinate $[Fe(III)]_2$ system in the literature, and magnetic measurements were not performed.[20] Instead, a comparison could be made for oxalate bridged Fe(III) compounds, where the metal ion is only hexacoordinate. In these cases, the values of the coupling constants were found to vary over the range –3.1 to –3.84 cm^{-1},[21-25] with the exception of the system $[Fe(bpm)_3]_2[Fe_2(ox)_5]\cdot 8H_2O$ (bpm = 2,2'-bipyrimidine), where the coupling between the dinuclear entities was found to measure –6.6 cm^{-1}, and remarked to be particularly strong.[26] Therefore, to complement the analytical fit of the magnetic data, the Estructura Electrònica group in the Departament de Química Inorgànica at the Universitat de Barcelona carried out DFT calculations to confirm the experimental results. The result was a calculated J value of –4.9 cm^{-1}, supporting that found through SQUID measurements (for more details on the calculations, see Appendix A1).

Compound	2	3	4	5	6	8	9
***T*/K**	150(2)	100(2)	100(2)	100(2)	150(2)	100(2)	100(2)
crystal system				Triclinic			
space group				P_{-1}			
***a*/Å**	13.185(3)	12.205(1)	11.980(1)	11.344(1)	12.046(1)	13.214(2)	13.518(2)
***b*/Å**	15.683(3)	13.386(1)	15.290(1)	12.751(1)	13.369(1)	15.801(3)	21.953(3)
***c*/Å**	17.460(4)	17.407(2)	18.743(1)	20.666(2)	18.099(1)	16.358(5)	23.588(3)
***α*/°**	105.50(3)	104.76(1)	104.866(1)	98.609(1)	108.03(1)	104.48(1)	106.32(1)
***β*/°**	100.50(3)	99.25(1)	98.796(1)	105.062(1)	101.60(1)	97.90(1)	105.30(1)
***γ*/°**	109.87(3)	105.12(1)	111.831(1)	90.757(1)	102.64(1)	110.56(1)	100.64(1)
***V*/Å^3**	3119.9(17)	2575.0(4)	2960.0(4)	2849.9(4)	2588.4(3)	2999.3(12)	6221.6(2)
***μ*/mm^{-1}**	0.403	0.599	0.526	0.538	0.483	0.419	0.501
Reflections collected	6521	12650	32810	23943	19209	14143	20810
***R*1 (all data)**	0.0748	0.0682	0.0603	0.0683	0.0823	0.0862	0.1048
***wR*2 (all)**	0.1822	0.1988	0.1883	0.2016	0.1945	0.2703	0.3237
S	0.76	1.04	1.07	1.079	1.019	1.055	1.14
av. Fe-N/Å	2.164	2.172	2.163	2.179	2.189	2.162	2.167
octahedral volume/Å^3	12.425	12.573	11.643	11.665	12.772	12.449	12.535
***Σ*/°**	148.54	146.27	171.12	184.92	152.63	142.20	141.23
***Φ*/°**	174.78(2)	176.96(2)	151.36(2)	146.71(2)	175.60(2)	174.88(2)	178.18
***θ*/°**	84.53	74.75	73.34	79.57	78.03	77.34	74.06
***Θ*/°**	471.35	460.83	501.97	523.91	492.75	466.44	451.69

Table 6.3: Crystallographic data and distortion parameters for compounds **2**, **3**, **4**, **5**, **6**, **8**, and **9**.

6.4 Single crystal X-ray diffraction study of compounds 2 and 3

Within the family of compounds presented in this Chapter, the majority form from a variation of the reaction medium with respect to the conditions employed in the synthesis of **1**. However, two compounds, **2** and **3**, are obtained from a procedure involving the ligand H_4L reacting with the perchlorate salt of Fe(II) in acetone. In the case of compound **2**, both the reaction medium and the precipitating agent (ether) are the same as for compound **1**; so it is therefore all the more surprising to observe the structural differences between the two systems. While both systems are based on an $[Fe(H_4L)_2]^{2+}$ cation, the rapidly forming complex **2** contains a molecule of diethyl ether in the lattice, three molecules of acetone, and none of water. The average Fe-N bond length for **2** is 2.164 Å,[27] corresponding to the Fe(II) centre in the HS state, which is also confirmed by the other structural parameters, θ, Φ, Σ, Θ (see Table 6.3).[28-31]

The most significant difference in the intermolecular interactions is the hydrogen bond established between a pyrazolyl ring of the H_4L ligand and a molecule of acetone (Figure 6.3, left). This situation is unusual for this family of compounds, in that only the counter-ion or a water molecule had been observed to occupy such a role. The angle formed by the atoms N1-O3S-C7S is 110.64°, where C7S is the central atom of the acetone molecule. The result is that the acetone molecule lies over the pyrazolyl ring of the ligand H_4L that is approximately perpendicular to that of N1. By blocking the faces of the wings of the $[Fe(H_4L)_2]^{2+}$ cation, one half of the expected face-to-face terpyridine embrace[32-34] interactions are prevented and the slight displacement of the distal phenol rings also causes the absence of the C-H$\cdots\pi$ contacts that otherwise reinforce the packing arrangement (Figure 6.3, right).

The situation found in compound **3** is perhaps more remarkable. It has the same composition as observed in **1** and, furthermore, the packing is based on the same mutual interactions between $[Fe(H_4L)_2]^{2+}$ cations, together with contacts involving the anions and solvents in the lattice. To illustrate this similarity, Figure 6.4 and Table 6.5 present the terpyridine embrace as observed in **3**. Comparison with Figure 4.2, shows that the strength and number of interactions is of the same order in both compounds. In fact, the differences between the two systems are to be encountered on a more subtle level. The average Fe-N bond length is longer in **3**, measuring 2.172 Å, compared to 2.162 Å in the HS structure of **1** at the same temperature (Table 6.3). However, to avoid any potential trapping of a meta-stable HS state, the sample had been cooled slowly from high

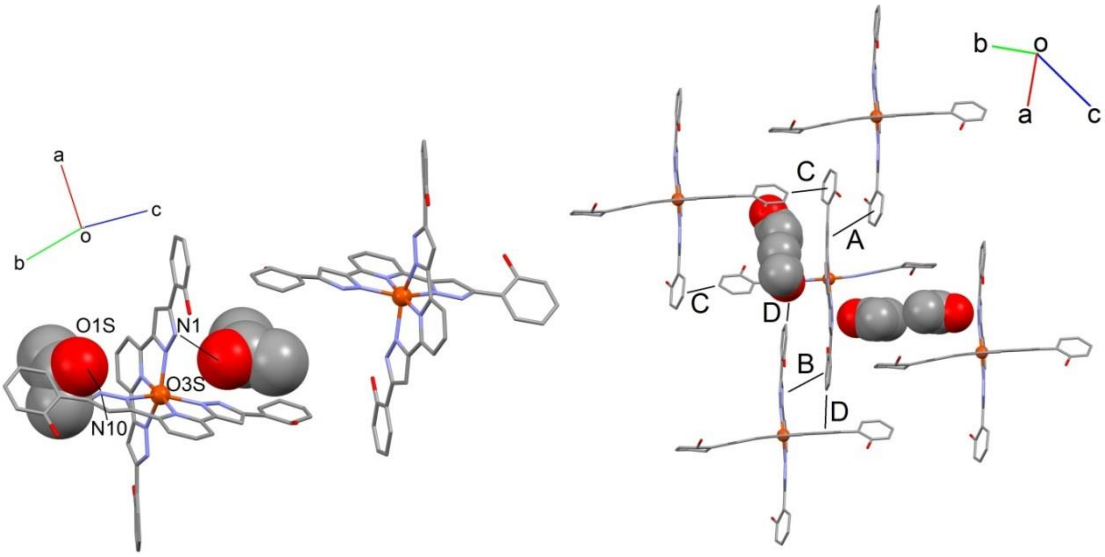

Contact	Labels	Distance/Å
H-bond	N1-H1···O3S	3.038(14)
H-bond	N10-H10···O1S	2.759(17)
π*···*π		
A	phen···pz	4.470
B	phen···pz	4.025
C-H···*π*		
C	C44-H44A···phen	3.866
D	C4-H4A···pz	3.890

Figure 6.3 and Table 6.4: (left) A representation of the direct hydrogen bonding of acetone molecules to the pyrazolyl rings of the $[Fe(H_4L)_2]^{2+}$ cations in **2**. (right) The effect of the acetone molecules on the terpy embrace, with the interactions given in the table. All hydrogen atoms are omitted for clarity.

temperatures. The level of order is also distinct. As in **1**, half of the perchlorate anions are disordered; however, there is a greater degree of disorder in **3**, with a higher mixed occupancy over two sites close to the pyridyl ring (0.6:0.4 in **3**, 0.8:0.2 in **1**). Additionally, the acetone molecules, both of which are split over two sites in **1**, are equally disordered in one case of **3**, and in the other the disorder could not be modelled.

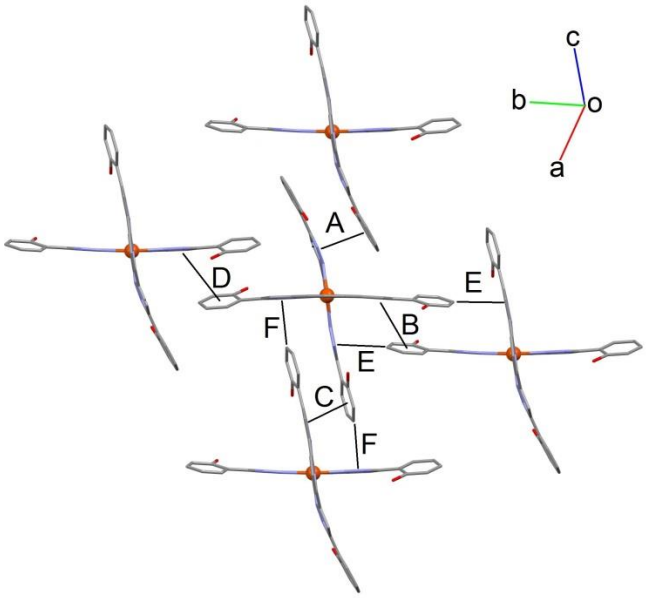

Contact	Labels	Distance/Å
π*···*π		100 K
A	pz···phen	3.596(2)
B	pz···phen	4.651(2)
C	pz···phen	4.096(2)
D	pz···phen	4.455(2)
C-H···*π*		
E	C21-H21A···pz	3.668(3)
F	C26-H26A···pz	3.384(3)

Figure 6.4 and Table 6.5: A representation of the co-planar cations in **3**, induced by *π*···*π* and C-H···*π* interactions. Hydrogen atoms are omitted for clarity. The table details the distances for each contact at 100 K, with centroids defined by PLATON.[35] pz = pyrazolyl ring, phen = phenol ring.

6.5 Magnetic properties of compounds 2 and 3

The magnetic properties of a dried powder sample of **2**, and a crystalline sample of **3**, are displayed in Figure 6.5. The measurement was then executed under an applied field of 5 kG, in a temperature range of 5-300 K, and is represented as the molar magnetic susceptibility product, χT, *vs*. the temperature, T, in Figure 6.5. At 300 K, χT = 3.32 (**2**) and 3.76 $cm^3mol^{-1}K$ (**3**), corresponding to Fe(II) in a HS state (χT = 3.00 $cm^3mol^{-1}K$ at 300 K for S = 2 and g = 2.0).[19] The slightly higher than expected value in the case of **3** is attributed to the effect of anisotropy observed on measuring a crystal sample, which can lead to higher than expected values of χT.[36] Decreasing the temperature at a rate of

1 Kmin^{-1} sees a near constant magnetic response, until the very lowest temperatures measured, where zero field splitting[37] causes a slight decline in χT. Therefore, both systems are observed to be HS over the range of temperatures measured.

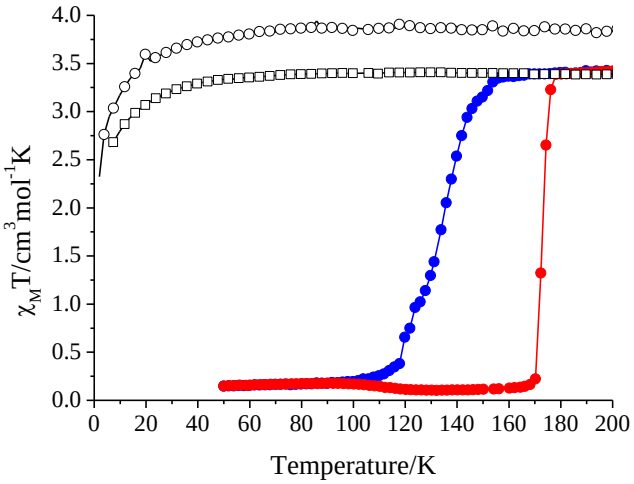

Figure 6.5: The molar magnetic susceptibility product, χT *vs*. the temperature, *T*, for **2** (squares) and **3** (white circles) in the temperature range 200 to 80 K, measured at a rate of 1 Kmin^{-1}. The magnetic properties of **1** are included for comparison.

For **2**, this absence of SCO behaviour with respect to compound **1** is apportioned to the rupture of the terpyridine embrace network of interactions, induced by the structural role played by solvent molecules. This was to prove a common motif in the rest of the systems based on changing the reaction conditions (see Section 6.6). The magnetic properties of **3** are more delicate to rationalise. The nearly identical structures of **1** and **3**, would allow the expectation of similar SCO phenomena. It could be proposed that the differing level of disorder in the crystal structure is at the root of this discrepancy. Because this disorder directly affects the intermolecular contacts with the pyrazolyl and pyridyl rings that chelate the Fe(II) ion, it may be that this is sufficient to alter any spin transition. The importance of crystallographic disorder in SCO systems was shown in Chapter 5, where distinct levels of disorder within one, unique system were shown to change the way in which excited states could access their common ground state.

6.6 Single crystal X-ray diffraction study of compounds 4, 5, 6, 8, and 9

The compounds **4**, **5**, **6**, **8**, and **9**, although they form in significantly different reaction conditions, are structurally related to **1**, with the differences between them caused by the

variation of solvent and anion employed in their syntheses. All five of these complexes crystallise in the triclinic P_{-1} space group (see Table 6.3), where the unit cell has two cations (**9** contains four, although is similar in all other ways), solvents depending on the synthesis, and the requisite anions to balance the charge. While **4**-**6** and **9** contain the expected $[Fe(H_4L)_2]^{2+}$ cation, **8** possesses a heteroleptic cation that features one neutral H_4L ligand and the anionic $H_2LBF_2^-$ moiety (see Figure 6.6). This variation does not affect the first coordination sphere, which is common to all five compounds, based on the chelation of the three central N-donor atoms from two 3-bpp derivatives, in an approximately perpendicular fashion. The average Fe-N bond lengths range from 2.162 to 2.189 Å, indicating five systems in the HS state. With respect to the central coordination pocket, all five systems contain one H_4L ligand with the phenol groups in a *syn,anti* conformation, with the exception of **8**, where the intact phenol group of $H_2LBF_2^-$ is disordered over both orientations (*anti*, 63%; *syn*, 37%).

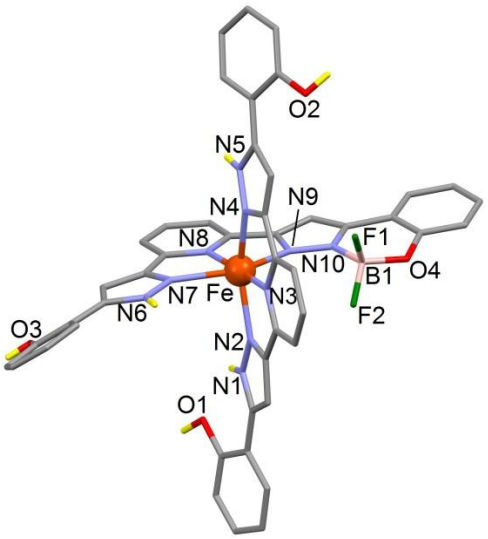

Bond	Bond length/Å
Fe-N3	2.105(4)
Fe-N8	2.133(5)
Fe-N2	2.173(5)
Fe-N4	2.190(5)
Fe-N7	2.209(5)
Fe-N9	2.160(5)
Average	2.162

Figure 6.6 and Table 6.5: A view of the $[Fe(H_4L)(H_2LBF_2)]^{2+}$ cation in **8**; hydrogen atoms omitted for clarity, except those bonded to heteroatoms, shown in yellow. The six Fe-N bond distances are given in the table.

Although the shape of these cations is similar to that in compound **1**, and favours the terpyridine embrace, the lattice solvent molecules are more active in intercalating within, and disrupting, the coplanar grids upon which the arrangement is based (Figure 6.7). In the case of **8**, there is a dual effect, where the formation of the five-membered heteroatomic C_3OBN ring impacts upon both the construction of the grids, and on the

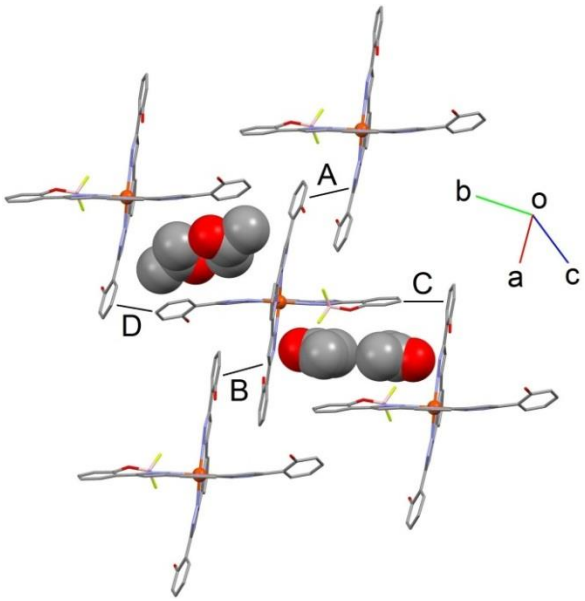

Contact	Labels	Distance/Å
π*···*π		
A	pz···phen	4.495(4)
B	pz···phen	4.229(3)
C-H···*π*		
C	C43-H43A···phen	3.640(9)
D	C26-H26A···phen	3.546(12)

Figure 6.7 and Table 6.6: A representation of the coplanar cations in **8**, induced by *π*···*π* and C-H···*π* interactions. Hydrogen atoms are omitted for clarity. The table details the distances for each contact, with the centroids defined by PLATON,[35] while pz = pyrazolyl and phen = phenol.

interaction between them. Because the cation is singly charged, only one tetrafluoroborate anion is required for charge balance, allowing the inclusion of more acetone molecules in the lattice. As a result, the crystal packing in **8** displays only half of the customary interactions for the embrace, due to the extra acetone molecules blocking two of the possible contacts between the wings. These molecules displace the terminal C-H groups of the phenol rings with respect to the pyrazolyl rings to which the C-H···*π* are usually established. Consequently, they are formed with the electron density on the distal phenol rings.

The planes formed by the cations, which are packed less efficiently due to the intervention of the acetone molecules, are linked through various interactions, mostly weak, that involve either the off-set *π*···*π* stacking of pyridyl rings, or hydrogen bonding of the ligand's wings conducted through the only tetrafluoroborate anion in the lattice

(Figure 6.8). The BF_2 fragment and the remaining phenol and pyrazolyl rings also establish intermolecular contacts, though again of a weak nature.

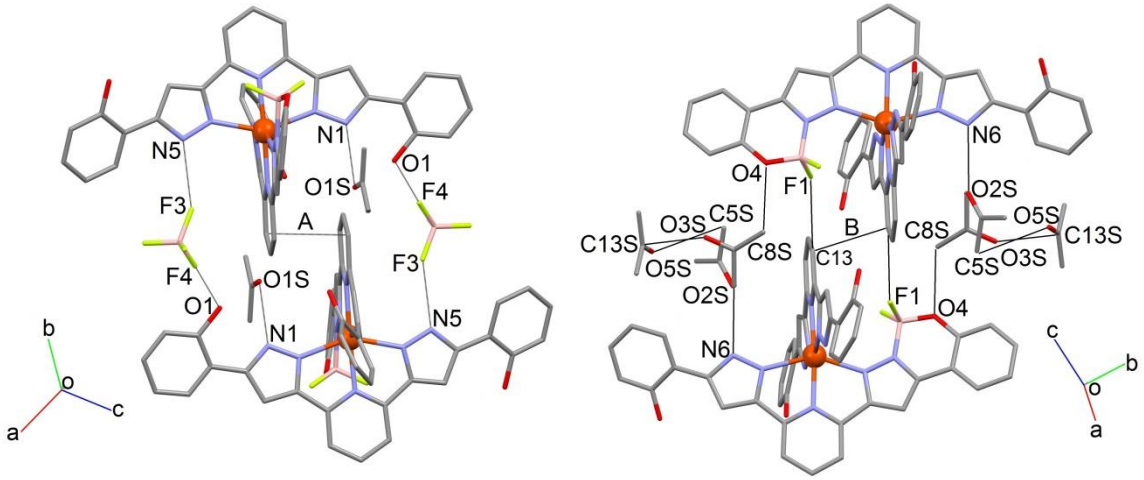

Contact	Distance/Å	Contact	Distance/Å
O1-H1···F4	2.752(6)	**N6-H6···O2S**	2.886(10)
N1-H1···O1S	2.970(6)	**O4···C8S**	3.40(3)
N5-H5···F3	2.820(6)	**O2S···O3B**	2.717(18)
		O3S···C13S	3.05(3)
		O5S···O3B	2.949(19)
		C12-H12···F1	3.082(6)
A = py···py	4.954(3)	**B = py···py**	4.954(2)
Fe···Fe	9.585(3)	**Fe···Fe**	10.114(3)

Figure 6.8 and Table 6.7: The hydrogen bonding motifs and metric parameters for the interactions that exist between the 2D layers in **8**, with hydrogen atoms omitted for clarity.

Compounds **4** and **5** both contain the $[Fe(H_4L)_2]^{2+}$ cation as seen in **1**, however, both systems are highly distorted in the first coordination sphere, as characterised by the parameter Φ. The packing forces within the crystal lattice of both of these complexes cause the severe deviation of Φ away from 180° to 151.4° and 146.7° for **4** and **5**, respectively (the cation of **4** is shown in Figure 6.9). These compounds are therefore the most distorted presented in this thesis, and are the most distorted to be found in the literature (see Chapter 9).

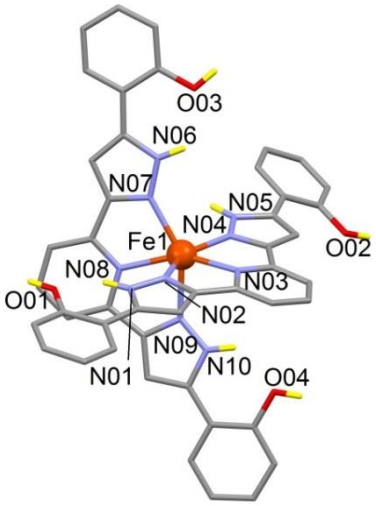

Bond	Bond length/Å
Fe-N03	2.146(2)
Fe-N08	2.143(2)
Fe-N02	2.197(2)
Fe-N04	2.155(2)
Fe-N07	2.152(2)
Fe-N09	2.186(2)
Average	2.163

Figure 6.9 and Table 6.8: A Mercury view of the $[Fe(H_4L)_2]^{2+}$ cations in **4**. The hydrogen atoms are omitted for clarity, except those bonded to heteroatoms, shown in yellow. The six Fe-N bond lengths are detailed in the table.

This distortion is attributed to the action of a perchlorate anion binding to one of the pyrazolyl rings in **4** (through N06, see Figure 6.10). This perchlorate anion, as well as bridging to the phenol ring of a neighbouring cation, establishes an anion$\cdots\pi$ supramolecular contact.[38] The effect of this is that, while the cations are maintained in contact, one of the H_4L ligands is moved towards one of the phenol groups (that of O04)

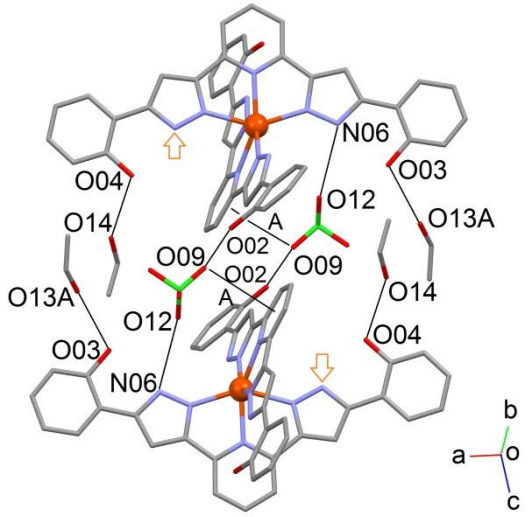

Contact	Distance/Å
N6-H6$\cdots$O12	3.097(6)
O3-H3$\cdots$O13A	2.86(1)
O4-H4$\cdots$O14	2.680(5)
O02-H2$\cdots$O09	2.858(5)
A = O09$\cdots$py	3.494(5)
Fe$\cdots$Fe	10.568(3)

Figure 6.10 and Table 6.9: The hydrogen bonding motifs and metric parameters for the interactions that exist between the layers in **4**, with hydrogen atoms omitted for clarity. Arrows indicate the blocked pyrazolyl ring.

which are part of the other H_4L ligand. This causes the pyrazolyl ring containing N10 to be sealed off, preventing their participation in any supramolecular interactions. The external phenol groups link to molecules of ethanol, accounting for two of the four lattice alcohol molecules.

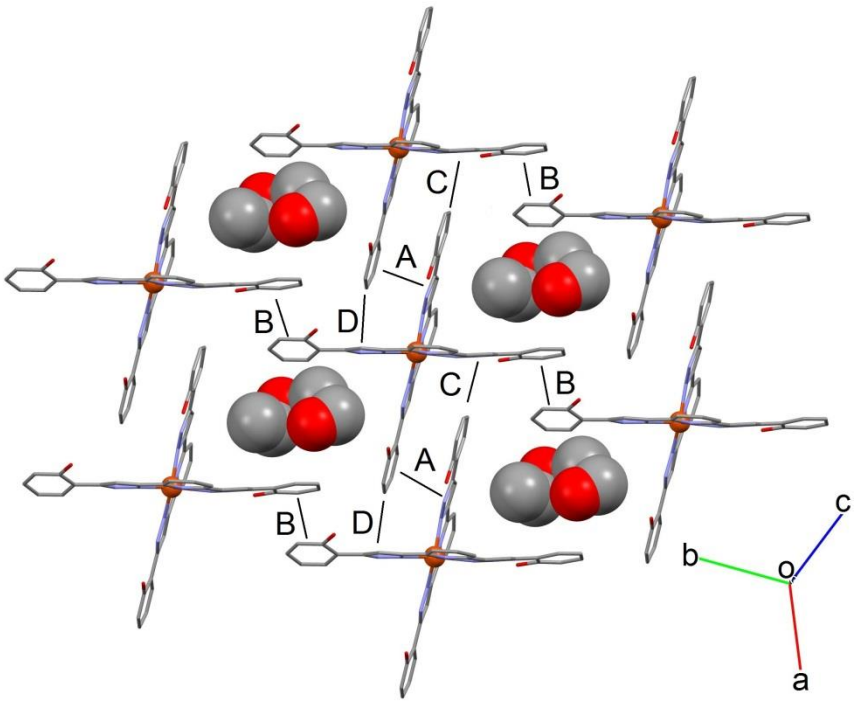

Contact	Labels	Distance/Å
π···π		
A	pz···phen	3.762(2)
B	phen···phen	3.790(3)
C-H···*π*		
C	C43-H44A···pz	3.741(4)
D	C26-H26A···pz	3.599(4)

Figure 6.11 and Table 6.10: The $\pi\cdots\pi$ and C-H$\cdots\pi$ motifs and metric parameters for the interactions that exist within the 2D layers in **4**, with hydrogen atoms omitted for clarity.

The remaining ethanol molecules are to be found within the co-planar grids, once again interrupting the potential overlap between neighbouring cations. In fact, only two "traditional" contact motifs from the terpyridine embrace are present: those where the pyrazolyl rings overlap with the phenol ring on a neighbouring cation, which are reinforced by C-H$\cdots\pi$ contacts, represented as the interactions A, C, and D, in Figure 6.11. The other contacts consist of more tenuous phenol···phenol motifs (B). The overall

displacement caused by these varied interactions results in the absence of pyridyl-to-pyridyl contacts, because the faces are not within sufficient proximity.

Compound **5** contains a similarly distorted cation, which is also induced by an anion···π contact.[38] However, in the case of **5**, there are only two solvent molecules (iso-propanol) in the lattice, with the consequence that they play a diminished role in the distortion that is analogous to that observed in **4** (c.f. Figure 6.10). Instead, the anion···π interaction and hydrogen bond to the pyrazolyl ring in which the perchlorate anions participate has the effect of bringing the anion closer to the centre of the $[Fe(H_4L)_2]^{2+}$ cation (Figure 6.12). This leaves space at the edge of the H_4L ligand to interact with a second perchlorate anion, and **5** is the only compound of this class which shows this unusual arrangement where both anions interact with the same wing of an H_4L ligand.

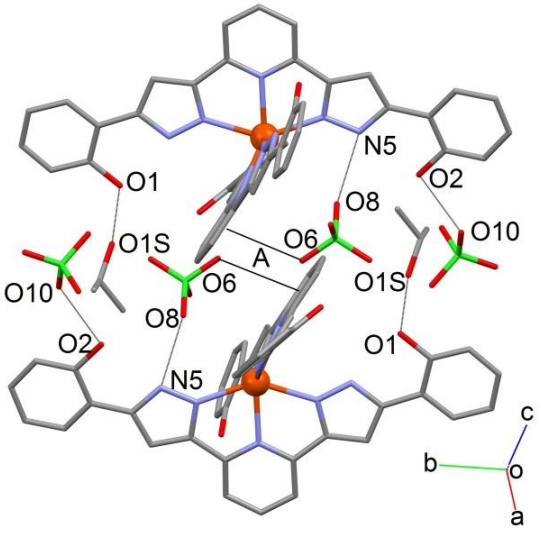

Contact	Distance/Å
O1-H1···O1S	2.675(8)
O2-H2···O10	2.766(7)
N5-H5···O8	2.984(8)
A = O6···py	3.445(5)
Fe···Fe	9.750(3)

Figure 6.12 and Table 6.11: The hydrogen bonding motifs and metric parameters for the interactions that exist between the coplanar layers in **5**, with hydrogen atoms omitted for clarity.

As well as distortion between the layers of the terpyridine embrace, there is also deformation of the embrace itself, where $[Fe(H_4L)_2]^{2+}$ cations participate in just three of the usual four interactions with nearest neighbour cations (Figure 6.13). The twist of one of the ligands with respect to the core of the cation, characterised by the value of Φ, also has the effect of displacing the terminal C-H groups of the distal phenol rings, resulting in an absence of C-H···π contacts in the lattice.

Given the modification enforced on the crystal packing of these previous compounds by the use of different solvents, the most "traditional" compound is therefore **6**, formed after slow evaporation of the mother liquor, nitromethane. The 2D grids are formed with the

full complement of interactions, both $\pi\cdots\pi$ and C-H$\cdots\pi$, a reflection of the regularity of the $[Fe(H_4L)_2]^{2+}$ cations, which display values of Φ of 175.60(2)°. These sheets are then connected through a network of intermolecular interactions, where the differences with respect to **1** are found.

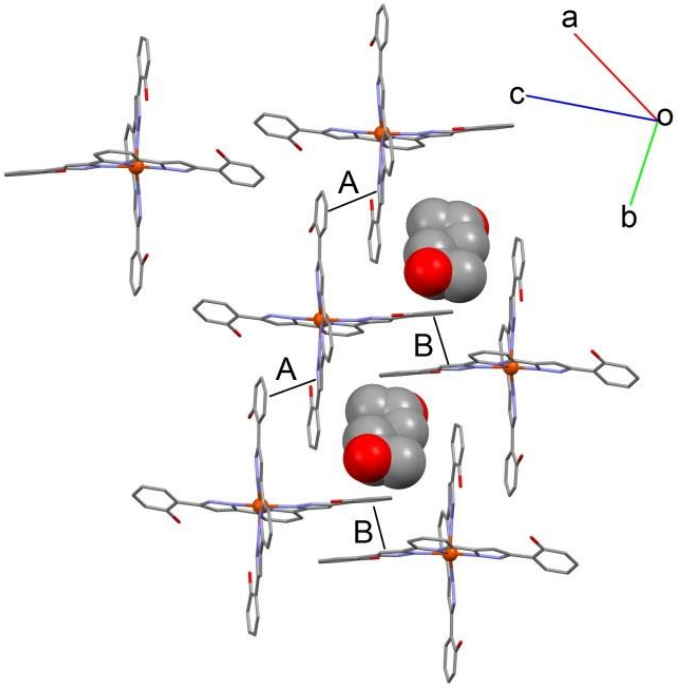

Contact	Labels	Distance/Å
π···π		
A	pz···phen	4.102(3)
B	pz···phen	3.691(3)

Figure 6.13 and Table 6.12 The $\pi\cdots\pi$ and C-H$\cdots\pi$ motifs and metric parameters for the interactions that exist within the coplanar layers in **5**, with hydrogen atoms omitted for clarity. The iso-propanol molecules are shown in the space-filling mode.

Here, the hydrogen bonding of water molecules to the pyrazolyl rings of adjacent cations pushes the perchlorate anions out, further away from the core of the compound. They then link to the distal phenol rings on the one side, and through a contact with a C-H bond to the other. The interaction of the water molecule directly with the pyrazolyl ring of 3-bpp derivatives has been discussed elsewhere, in terms of its possible effect on the spin state of Fe(II) systems. It was suggested that this interaction could increase the basicity of the ligand, and therefore stabilise the LS state,[39, 40] although this is found to be contrary to the case of **6**.

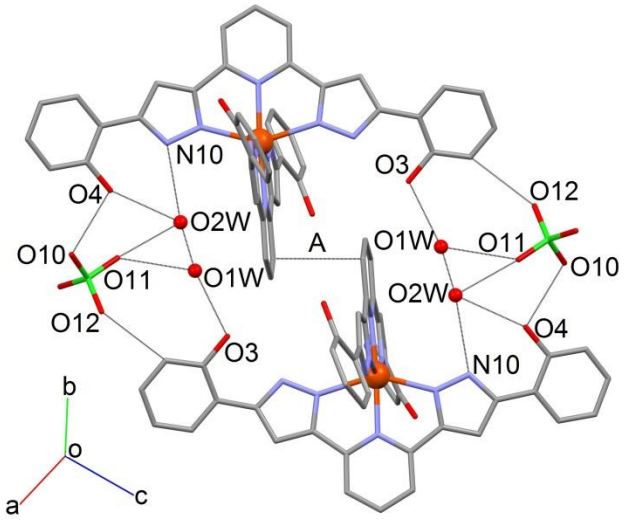

Contact	Distance/Å
O3-H3···O1W	2.674(9)
O4-H4···O2W	2.884(8)
O4-H4···O10	2.743(8)
N10-H10···O2W	2.948(9)
O11···O1W	2.919(8)
O1W···O2W	2.715(10)
A = py···py	4.751(3)
Fe···Fe	9.793(3)

Figure 6.14 and Table 6.13: The hydrogen bonding motifs and metric parameters for the interactions that exist between the coplanar layers in **6**, with hydrogen atoms omitted for clarity. The H_2O molecules are represented in ball and stick form.

Compound **9** contains the triflate anion, which is involved in a mechanism similar to the perchlorate anion for bridging between cations (Figure 6.15). The triflate ion, however, is substantially bulkier than the perchlorate, because of the trifluoromethyl group which takes the place of what would be a terminal oxygen in the case of ClO_4^-. Here, the anion forms a hydrogen bond with the pyrazolyl ring of the $[Fe(H_4L)_2]^{2+}$ through the terminal fluoride of the trifluoromethyl group. Analogously to the action of the acetone molecules in **2** (c.f. Figure 6.3), due to an anion···π interaction between a terminal oxygen atom and the pyrazolyl ring of the H_4L ligand, the bulky sulphite group lies along the H_4L ligand which is perpendicular to that of the hydrogen-bonding pyrazolyl ring. These anions, together with solvent acetone molecules, interrupt the terpyrdine embrace (Figure 6.15, right). The steric bulk of both entities, anion and solvent molecule, results in the aromatic wings of the ligand being unable to approach the rings from adjacent complexes favourably on all four extremities of the cations. Further, those wings which do interact show a single phenol···phenol contact, which is not reinforced by participation of the pyrazolyl rings.

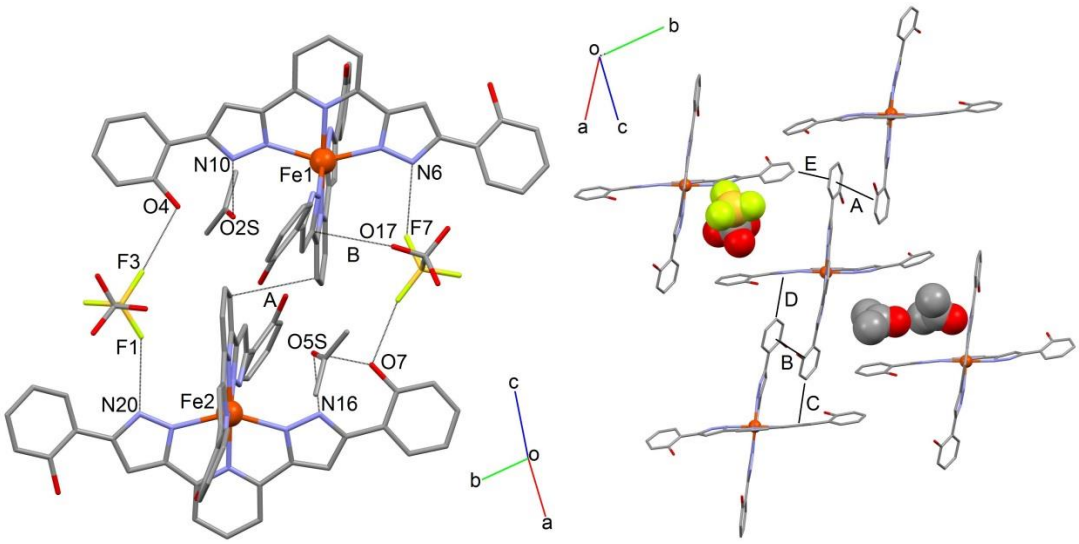

Contact	Distance/Å	Contact	Distance/Å
left		**right**	
N6-H6···F7	2.785(5)	**A = phen···phen**	4.052(3)
N10-H10···O2S	2.891(6)	**B = phen···phen**	3.652(3)
N16-H16···O5S	2.974(6)	**C = C49-H49A···pz**	3.712(5)
N20-H20···F1	2.880(5)	**D = C21-H21A···pz**	3.656(5)
O4-H4···F3	2.773(6)	**E = C26-H26A···phen**	3.637(6)
O7-H7···F9	2.710(6)		
A = **py···py**	4.867(2)		
B = **O17···pz**	3.248(5)		

Figure 6.15 and Table 6.14: (left) A representation of the direct hydrogen bonding of acetone molecules to the pyrazolyl rings of the $[Fe(H_4L)_2]^{2+}$ cations and hydrogen bonding between layers in **9**. (right) The effect of the acetone molecules and triflate anions on the terpy embrace, with the interactions given in the table. All hydrogen atoms are omitted for clarity.

6.7 Magnetic properties of compounds 4, 5, 6, 8, and 9

Magnetic susceptibility measurements were carried out on polycrystalline samples of compounds **4**, **5**, **6**, **8**, and **9** which had been briefly dried in air, in the temperature range 5-300 K under an applied field of 5 kG (Figure 6.16). At 300 K, the compounds show values of χT of 3.67 (**4**), 3.83 (**5**), 3.91 (**6**), 3.34 (**8**), and 3.60 $cm^3mol^{-1}K$ (**9**) due to Fe(II) ions in the HS state (χT = 3 $cm^3mol^{-1}K$ for S = 2, supposing g = 2.0). Lowering the temperature at 1 $Kmin^{-1}$, sees an almost constant magnetic response in all the compounds, until around 50 K, where the values of χT start to decrease due to zero field splitting

effects, giving χT = 2.59, 2.09, 2.14, 2.00, and 3.16 $cm^3mol^{-1}K$ for **4**, **5**, **6**, **8**, and **9** respectively, at the lowest temperatures measured. These data are consistent with five systems that remain in the HS state over the temperature range measured, and with the single crystal structures as resolved via diffraction studies.

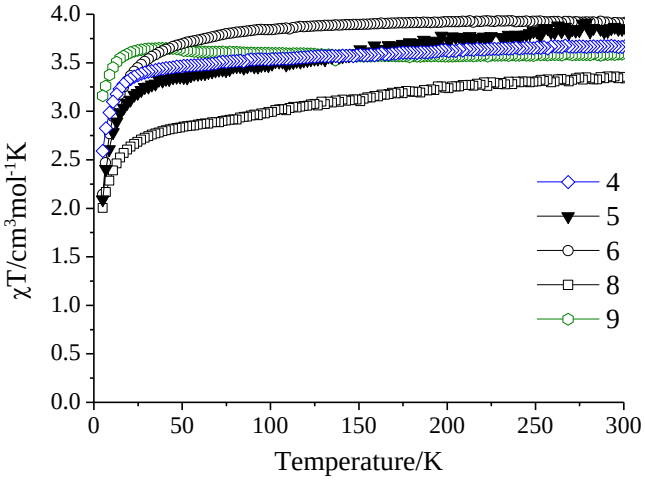

Figure 6.16: A graph of χT *vs*. the temperature, *T*, for compounds **4**, **5**, **6**, **8**, and **9** in the range 300 to 5 K, measured at a rate of 1 $Kmin^{-1}$.

6.8 Concluding remarks

By varying the synthetic parameters that were employed to yield **1**, eight novel compounds were obtained. Each, in their own way, illustrates the delicate nature of SCO with respect to the approach taken to the synthesis of a given family of systems.

In the case of **2**, the kinetic product of the reaction that produces **1**, the precipitating agent (diethyl ether) is involved in the formation of the crystal lattice, and the acetone molecules participate in direct hydrogen bonding to the $[Fe(H_4L)_2]^{2+}$ cations. The subsequent effect is that solvent molecules interrupt the terpyridine embrace in which **1** crystallises. This was also observed in compounds **4** and **5**, and in all three systems, this less efficient packing was deemed to be one of the deciding factors in the lack of SCO. The cations in compound **6**, obtained from nitromethane, present interactions between the pyrazolyl rings of the H_4L ligand and two water molecules. This is shown to push the perchlorate anions away from their favoured position of linking the pyrazolyl ring of one cation with the phenol ring of an adjacent cation, thought to lead to the HS only behaviour measured in the SQUID.

If, rather than diethyl ether, dichloromethane is used to crystallise the product of the reaction that yields **1**, then system **3** is formed. This compound is shown to be the most similar to **1**, and is in fact virtually indistinguishable in terms of hydrogen bonding motifs and crystal packing. Closer inspection shows that there is a difference in the level of disorder in the lattice, both in the acetone molecules, and in the perchlorate anions. The result of this extremely subtle difference in packing is an increased Fe-N bond length around the Fe(II) core. The morphology of the crystals is markedly different, with the large polycrystalline aggregates that compose **1** contrasting sharply with the discrete monocrystals of **3**. A combination of these factors is proposed as the cause of the absence of SCO in **3** when, *a priori*, its structure could have given the strongest possibility of a transition.

Changing the charge-balancing anion from perchlorate to the structurally analogous tetrafluroborate anion demonstrated an unexpected reactivity of the H_4L ligand. This led to the heteroleptic complex **8**, based on the mono-cation $[Fe(H_4L)(H_2LBF_2)]^+$. Although this compound also displays a modified form of the terpyridine embrace, it is difficult to make a direct comparison with magnetic properties of the other compounds presented, due to the coordination of an anionic ligand to the Fe(II) centre. The observation of the fluoroborated derivative of H_4L led to the development of the ligand H_2L1 (see Chapter 8), which contains methoxy- rings attached to the 3-bpp core, rather than the hydroxy- rings of H_4L.

The importance of the weakly coordinating character of ClO_4^- anions in the majority of these systems was illustrated by the formation of the dinuclear Fe(III) compound **10**. Use of an anion like thiocyanate, sees the coordination of H_4L in the equatorial positions of the metal centre, with the anion binding axially. Presumably, the stability of the final assembly is what then drives the oxidative cleavage of the ascorbic acid, which had been used to avoid the oxidation of Fe(II) to Fe(III). This process provided the oxalate bridge that links the two metal centres and, rather than SCO phenomena, magnetic superexchange is observed.

6.9 References

1. R. Nowak, W. Bauer, T. Ossiander and B. Weber, *Eur. J. Inorg. Chem.*, 2013, **2013**, 975-983.
2. P. N. Martinho, Y. Ortin, B. Gildea, C. Gandolfi, G. McKerr, B. O'Hagan, M. Albrecht and G. G. Morgan, *Dalton Trans.*, 2012, **41**, 7461-7463.
3. B. Li, R. J. Wei, J. Tao, R. B. Huang, L. S. Zheng and Z. P. Zheng, *J. Am. Chem. Soc.*, 2010, **132**, 1558-1566.
4. R. Pritchard, H. Lazar, S. A. Barrett, C. A. Kilner, S. Asthana, C. Carbonera, J.-F. Letard and M. A. Halcrow, *Dalton Trans.*, 2009, 6656-6666.
5. S. Bonnet, G. Molnár, J. S. Costa, M. A. Siegler, A. L. Spek, A. Bousseksou, W. T. Fu, P. Gamez and J. Reedijk, *Chem. Mat.*, 2009, **21**, 1123-1136.
6. W. Zhang, F. Zhao, T. Liu, M. Yuan, Z.-M. Wang and S. Gao, *Inorg. Chem.*, 2007, **46**, 2541-2555.
7. M. C. Giménez-López, M. Clemente-León, E. Coronado, F. M. Romero, S. Shova and J.-P. Tuchagues, *Eur. J. Inorg. Chem.*, 2005, 2783-2787.
8. Y. Hasegawa, R. Sakamoto, K. Takahashi and H. Nishihara, *Inorg. Chem.*, 2013, **52**, 1658-1665.
9. D. Sertphon, D. J. Harding, P. Harding, K. S. Murray, B. Moubaraki, J. D. Cashion and H. Adams, *Eur. J. Inorg. Chem.*, 2013, 788-795.
10. H. S. Scott, T. M. Ross, B. Moubaraki, K. S. Murray and S. M. Neville, *Eur. J. Inorg. Chem.*, 2013, 803-812.
11. C. J. Schneider, J. D. Cashion, N. F. Chilton, C. Etrillard, M. Fuentealba, J. A. K. Howard, J.-F. Létard, C. Milsmann, B. Moubaraki, H. A. Sparkes, S. R. Batten and K. S. Murray, *Eur. J. Inorg. Chem.*, 2013, 10.1002/ejic.201201075.
12. A. M. McDaniel, C. M. Klug and M. P. Shores, *Eur. J. Inorg. Chem.*, 2013, 943-950.
13. X. Bao, J. D. Leng, Z. S. Meng, Z. J. Lin, M. L. Tong, M. Nihei and H. Oshio, *Chem.-Eur. J.*, 2010, **16**, 6169-6174.
14. M. Clemente-León, E. Coronado, M. Carmen Giménez-López, F. M. Romero, S. Asthana, C. Desplanches and J.-F. Létard, *Dalton Trans.*, 2009, 8087-8095.
15. R.-J. Wei, J. Tao, R.-B. Huang and L.-S. Zheng, *Eur. J. Inorg. Chem.*, 2013, 916-926.
16. R.-J. Wei, J. Tao, R.-B. Huang and L.-S. Zheng, *Inorg. Chem.*, 2011, **50**, 8553-8564.
17. P. Zhou, Y.-G. Zhao, Y. Bai, K.-L. Pang and C. He, *Inorg. Chim. Acta*, 2007, **360**, 3965-3970.
18. G. de Ruiter, J. S. Costa, K. Lappalainen, O. Roubeau, P. Gamez and J. Reedijk, *Inorg. Chem. Commun.*, 2008, **11**, 787-790.
19. O. Kahn, *Molecular Magnetism, Wiley VCH*, 1993.
20. H. Aghabozorg, F. Ramezanipour, J. Soleimannejad, M. A. Sharif, A. Shokrollahi, M. Shamsipur, A. Moghimi, J. A. Gharamaleki, V. Lippolis and A. J. Blake, *J. Pol. Chem.*, 2008, **82**, 487.
21. E. Safaei, T. Weyhermüller, E. Bothe, K. Wieghardt and P. Chaudhuri, *Eur. J. Inorg. Chem.*, 2007, 2334-2344.
22. D. Armentano, G. De Munno, F. Lloret and M. Julve, *CrystEngComm*, 2005, **7**, 57-66.
23. S. Triki, F. Berezovsky, J. Sala Pala, E. Coronado, C. J. Gómez-García, J. M. Clemente, A. Riou and P. Molinie, *Inorg. Chem.*, 2000, **39**, 3771-3776.

24. S. Rashid, S. S. Turner, P. Day, M. E. Light and M. B. Hursthouse, *Inorg. Chem.*, 2000, **39**, 2426-2428.
25. E. Coronado, J. R. Galán-Mascarós and C. J. Gomez-Garcia, *J. Chem. Soc., Dalton Trans.*, 2000, 205-210.
26. D. Armentano, G. De Munno, J. Faus, F. Lloret and M. Julve, *Inorg. Chem.*, 2001, **40**, 655-660.
27. A. Hauser, *Top. Curr. Chem.*, 2004, **233**, 49-58.
28. P. Guionneau, M. Marchivie, G. Bravic, J.-F. Létard and D. Chasseau, *Top. Curr. Chem.*, 2004, **234**, 97-128.
29. J. M. Holland, J. A. McAllister, C. A. Kilner, M. Thornton-Pett, A. J. Bridgeman and M. A. Halcrow, *J. Chem. Soc. Dalton Trans.*, 2002, 548-554.
30. J. K. McCusker, A. L. Rheingold and D. N. Hendrickson, *Inorg. Chem.*, 1996, **35**, 2100-2112.
31. M. G. B. Drew, C. J. Harding, V. McKee, G. G. Morgan and J. Nelson, *J. Chem. Soc., Chem. Commun.*, 1995, 1035-1038.
32. J. McMurtrie and I. Dance, *CrystEngComm*, 2005, **7**, 216-229.
33. K. H. Sugiyarto, M. L. Scudder, D. C. Craig and H. A. Goodwin, *Aust. J. Chem.*, 2000, **53**, 755-765.
34. M. L. Scudder, H. A. Goodwin and I. G. Dance, *New J. Chem.*, 1999, **23**, 695-705.
35. A. L. Spek, *J. App. Cryst.*, 2003, **36**, 7-13.
36. S. Bonnet, M. A. Siegler, J. S. Costa, G. Molnár, A. Bousseksou, A. L. Spek, P. Gamez and J. Reedijk, *Chem. Commun.*, 2008, 5619-5621.
37. M. A. Halcrow, *Chem. Soc. Rev.*, 2008, **37**, 278-289.
38. T. J. Mooibroek, C. A. Black, P. Gamez and J. Reedijk, *Cryst. Growth Des.*, 2008, **8**, 1082-1093.
39. T. D. Roberts, F. Tuna, T. L. Malkin, C. A. Kilner and M. A. Halcrow, *Chem. Sci.*, 2012, **3**, 349-354.
40. S. A. Barrett, C. A. Kilner and M. A. Halcrow, *Dalton Trans.*, 2011, 12021-12024.